Impact of Diffuse Radiation Modeling on Rear/Front Ratio Estimation for Bifacial PV Systems

Joao V. F. F. Medeiros[1,3], Janis J. B. Galdino[1], Rinaldo O. Melo[1], Rodrigo Alonso-Suárez[2] and Olga C. Vilela[1]

[1] Center for Renewable Energy (CER), Federal University of Pernambuco (UFPE), Recife (Brazil)

[2] CENUR Litoral Norte, Universidad de la República, Salto (Uruguay)

[3] Recurrent Energy Power Systems, São Paulo (Brazil)

Abstract

The accurate modeling of diffuse irradiance is essential for evaluating the rear/front ratio (R/F) in bifacial photovoltaic (PV) systems. This study investigates the performance of different diffuse separation and transposition models for front and rear irradiance estimation using field data collected in Recife, Brazil (8°S, 34°W). Two separation models (Erbs and Starke3) and two transposition models (Isotropic and HDKR) were tested in their four possible combinations. Results show that the Starke3 model consistently outperforms Erbs in estimating both global (GTI) and rear (RTI) tilted irradiances. When combined with the HDKR model, Starke3 achieved the lowest normalized mean absolute error for the rear tilted irradiance (13.8% for RTI) and the best agreement with observed R/F ratios. The HDKR model improved R/F estimations by reducing nRMSE from 24.2% to 19.9%. The study demonstrates that accurate diffuse modeling, especially under medium to high clearness index conditions, is crucial to properly quantify rear irradiance and consequently the bifacial gains. Neglecting anisotropy or horizon brightening can increase the R/F estimation errors, significantly affecting the bifacial gain estimation error in 40%.

Keywords: albedo, rear/front ratio, rear irradiance, bifacial gain, diffuse irradiance, GHI separation, transposition model

1. Introduction

Bifacial photovoltaic (PV) modules account for approximately 90% of current global PV module sales, a share that is expected to remain stable over the next 10 years (VDMA, 2024). The bifacial modules' ability to capture solar irradiance on both the front and rear surfaces increases energy production potential compared to the traditional front-only collecting modules. The annual yield gains can increase up to 10%, even for fixed-tilt ground-mounted systems ,with a typical natural ground cover albedo of 0.25 (Sun et al., 2018).

Reliable estimation of bifacial PV performance depends heavily on accurate modelling of the diffuse irradiance reaching both sides of a tilted surface. While ray tracing tools such as RADIANCE (Ward, 1994) provide detailed simulations, the computationally intensive nature of these tools limits their use in typical applications, making diffuse irradiance factor-based methods more practical for modeling bifacial systems (Marion et al., 2017). However, these approaches rely on the accurate transposition of diffuse irradiance from horizontal to tilted surfaces, and in the absence of direct/diffuse measurements, they also rely directly on global horizontal (GHI) decomposition models.

The complexity of bifacial PV modeling has been investigated in recent literature, with particular emphasis on

the challenges associated with rear surface irradiance estimation. Deline et al. (2024) demonstrated that tilted diffuse factor-based approaches can achieve reasonable accuracy for bifacial systems performance assessment when the inputs are global and diffuse horizontal measurements, but may present significant variability under specific conditions such as snowy events. Similarly, Asgharzadeh et al. (2019) implemented global and diffuse measurements to compare the performance of 2D and 3D view factors, the authors highlighted that 2D view factors are sufficiently accurate to estimate annual energy for any well-characterized bifacial PV system. Recent advances in decomposition modeling, such as those presented by Starke et al. (2021), have introduced enhanced meteorological sensitivity that could potentially improve bifacial performance predictions when diffuse measurements are not available. However, the specific impact of different decomposition and transposition model combinations on rear/front ratio estimation or on bifacial gain remains insufficiently explored, particularly regarding their relative performance under varying atmospheric conditions.

In this context, the present study investigates the influence of two global horizontal irradiance decomposition models (Erbs and Starke3) and two diffuse transposition models (Isotropic and HDKR) on the estimation of tilted irradiance components, including both reflected and sky dome diffuse irradiance. The analysis aims to assess their impact on the rear/front irradiance ratio for bifacial PV systems.

2. Diffuse modelling

To estimate the global or rear tilted irradiances is fundamental to have all horizontal components. When direct normal irradiance (DNI) and diffuse horizontal irradiance (DHI) measurements are not available, which is a common situation worldwide, GHI separation models must be implemented to separate global horizontal irradiance into its direct and diffuse components (Starke et al., 2018).

One of the most widely used empirical models is the Erbs model (Erbs et al., 1982). In the present paper it is used as a baseline for estimating the diffuse fraction (kd) and consequently the DHI and DNI. The Erbs model is a simple and univariate model based on the clearness index (kt) (see eq. 1).

The Starke3 model (Starke et al., 2021) represents a significant advancement in high resolution diffuse fraction modeling by incorporating multiple meteorological and temporal variables. This model introduced several improvements over previous approaches, like the BRL model (Ridley et al, 2010) or STARKE2 (Starke et al., 2018).

$$k_d^{\boldsymbol{ERBS}} = \begin{cases} 1 - 0.09k_t & k_t \leq 0.22 \\ 0.9511 - 1.1605k_t + 4.388k_t^2 - 16.638k_t^3 + 12.336k_t^4 & 0.22 < k_t \leq 0.8 \\ 0.177 & k_t > 0.8 \end{cases} \quad \text{(eq. 1)}$$

$$k_d^{\boldsymbol{STARKE3}} = \begin{cases} \frac{1}{\left[1+\exp\left(\beta_8+\beta_9 k_t+\beta_{10}HSA+\beta_{11}\alpha+\beta_{12}K_t+\beta_{13}\psi+\beta_{14}\frac{CSI}{277,78}+\beta_{15}k_{t,h}\right)\right]}, & K_{CSI} < 1{,}05 \\ \frac{1}{\left[1+\exp\left(\beta_0+\beta_1 k_t+\beta_2 HSA+\beta_3\alpha+\beta_4 K_t+\beta_5\psi+\beta_6\frac{CSI}{277,78}+\beta_7 k_{t,h}\right)\right]}, & K_{CSI} \geq 1{,}05 \; e \; k_t > 0{,}75 \end{cases} \quad \text{(eq. 2)}$$

where k_t = GHI/G_{0h} represents the clearness index, with G_{0h} being the extraterrestrial horizontal irradiance. The variability index (ψ) captures the temporal variability of solar irradiance, providing better estimates during intermittent cloud conditions. The hourly clearness index ($k_{t,h}$) describes low-frequency variations, like a variability index but with lower variations. Other parameters like the solar elevation angle (α), apparent solar time (AST), daily clearness index (K_t) and the clear sky irradiance (CSI) obtained based on the simplified Solis model (Ineichen, 2008) are also used to improve the model's responsiveness to short-term atmospheric changes, notably the cloud enhancement events. The coefficients (β) presented in eq. 2 are derived from Starke et al. (2021), where the model is calibrated for different climates, in the present paper the coefficients of the Tropical climate were selected.

Once horizontal irradiance components are available, the global tilted irradiance (GTI) and the rear tilted irradiance (RTI) can be estimated by the sum of the direct and diffuse irradiance incident on the inclined plane. The diffuse irradiance over each plane is composed of the irradiance that comes from sky-dome, excluding directions of the Sun's disk, and the irradiance that is reflected by the ground. These both contribute to diffuse irradiance on each side of the module through the way they are seen by each surface. The transposition of direct irradiance is straightforward and obtained through geometric conversion, considering the angle of incidence between the solar beam and each surface (front, AI_{front} and rear, AI_{rear}). The transposition of diffuse irradiance is considerably more complex due to the anisotropic nature of sky radiance distribution. The reflected component is typically treated with simplified approaches given its relatively lower contribution to the total irradiance budget and is represented as the product of the reflected horizontal irradiance (RTI, calculated as GHI times the albedo) and a simple Ground View Factor (GVF). In contrast, sky-dome diffuse irradiance has been modelled with more complex expressions multiplying DHI, for instance, treating some of the circumsolar diffuse as direct and including horizon sky-dome brightening. By conveniently defining a Tilted Diffuse Ratio (TDR) modelling the the sky dome diffuse irradiance, all the transposition models considered in this study can be written as follows:

$$GTI = DNI\ cos(AI_{front}) + DHI * TDR_{front} + RHI * GVF_{front} \quad \text{(eq. 3)}$$

$$RTI = DNI\ cos(AI_{rear}) + DHI * TDR_{rear} + RHI * GVF_{rear} \quad \text{(eq. 4)}$$

Diffuse transposition models can be classified into two main categories: isotropic models, which assume uniform sky radiance distribution, and anisotropic models, which account for the non-uniform distribution of diffuse radiation across the sky dome. The isotropic model of Liu and Jordan (1961) represents the simplest approach, assuming uniform sky brightness and therefore a simple Sky View Factor (SVF) is enough to model the sky dome diffuse irradiance contribution. The TDR for front and rear are then represented by eq. 5 and 6.

$$TDR_{front} = SVF_{front,iso} = \frac{1+\cos\beta}{2} \quad \text{(eq. 5)}$$

$$TDR_{rear} = SVF_{rear,iso} = \frac{1-\cos\beta}{2} \quad \text{(eq. 6)}$$

The model proposed by Reindl et al. (1990) extends previous diffuse irradiance formulations by adding a horizon brightening term to better represent sky conditions. It builds on the work of Hay and Davies (1980), who introduced the anisotropy index to differentiate isotropic sky dome diffuse radiation from the circumsolar diffuse radiation. Earlier, Temps and Coulson (1977) and Klucher (1979) had refined the isotropic assumption by including horizon brightness and developing an all-sky modulating function. The combined contributions of these studies form what is widely known as the HDKR model (Duffie and Beckman, 2013). The eq. 7 represents the TDR of the HDKR model and eq. 6 is an adaptation of this model to the rear side.

$$TDR_{front,HDKR} = \left[F_{HD}R_{b,front} + (1 - F_{HD})\left(\frac{1-\cos\beta}{2}\right)\left(1 + f\sin^3\left(\frac{\beta}{2}\right)\right)\right] \quad \text{(eq. 7)}$$

$$TDR_{rear,HDKR} = \left[F_{HD}R_{b,rear} + (1 - F_{HD})\left(\frac{1+\cos\beta}{2}\right)\left(1 + f\sin^3\left(\frac{180-\beta}{2}\right)\right)\right] \quad \text{(eq. 8)}$$

where R_b is the geometric factor for the front ($R_{b,front}$) and rear side ($R_{b,rear}$), F_{HD} is the anisotropy index of Hay and Davies calculated by DNI/DNI_{ext}, where DNI_{ext} is the extraterrestrial direct normal irradiance and f is the

modulation factor of Reindl represented as $\sqrt{DNI \cos\theta_z / GHI}$).

For the reflected component the assumption of uniform reflected radiance distribution is applied with a global albedo value modeling the ground reflectance. The view factor to estimate tilted irradiance (both front and back) can be adjusted by a distribution function of elevation (Durusoy et al., 2020) as the PV module experiences different irradiance levels at different highs (top and bottom of the module). For this study, as the RTI and GTI measurements are recorded by sensors on the same level, these more complex functions are not applied. The ground view factor for both front and rear are calculated by eq. 9.

$$GVF_{front} = \frac{1-\cos\beta}{2} \quad ; \quad GVF_{rear} = \frac{1+\cos\beta}{2} \qquad \text{(eq. 9)}$$

3. Data and Methodology

The experimental data were collected at the Center for Renewable Energy (CER-UFPE) in Recife, Brazil (8.055°S, 34.955°W, 4 m elevation), characterized by a Tropical Monsoon climate (Köppen–Geiger: Am). Global and reflected horizontal irradiances were measured using an EKO MS-60 albedometer (305–2800 nm, Class B according to the ISO 9060:2018 standard), while tilted front and rear irradiance data were obtained from two Li-Cor Li-200R pyranometers (400–1100 nm), calibrated with a Kipp & Zonen CMP22 secondary standard. All sensors were mounted 2 meters above ground level (see Fig. 1).

Fig. 1: Weather station with horizontal albedometer and tilted sensors at 30°.

The methodology begins with the acquisition and quality control of solarimetric data. Standard filters from Rodríguez-Muñoz et al. (2024) and Baseline Surface Radiation Network (BSRN) (McArthur, L., 2005) were applied, along with an additional filter to exclude shading effects from a nearby experimental tower. All filters were applied to the global tilted and horizontal irradiance in the two directions (front and back). The filters from BSRN related to the diffuse component were applied in this work as an upper limit for the rear irradiance components (RTI and RHI) as these components are highly influenced by the reflection on the ground and may have values below the BSRN threshold.

The filters related to Albedo were applied based on Rodríguez-Muñoz et al. (2024), but the statistical filter of albedo envelope was adapted from a 3σ threshold toa more conservative value of 2σ, motivated from Petribu et al. (2017) when removing outliers for the diffuse fraction.

As a summary, the filters applied on the quality control procedure are:

- Physical Limits: $0\ W/m^2 < GTI, GHI, RHI, RTI < 2000\ W/m^2$
- BSRN Limits: $0\ W/m^2 < GTI, GHI < S_c\ p\ (\cos\theta_z)^a \quad \therefore \quad S_c = 1361.1\ W/m^2$, p = 1.5, a = 1.2
  $0\ W/m^2 < RHI, RTI < S_c\ p\ (\cos\theta_z)^a \quad \therefore \quad S_c = 1361.1\ W/m^2$, p = 0.95, a = 1.2
- k_t limits: $0 < k_t < 1.4$
- Solar elevation: $\theta_z < 83°$
- Albedo limits: $0 \leq \rho_g \leq 1$
- Albedo Envelope: $|\rho_g - \bar{\rho}_g| \leq 2\sigma$,
- Shading removal: $\gamma \notin [\gamma_A, \gamma_B]$ and $\alpha \geq \alpha_{A|B}$

The last filter, related to shading removal, was based on geometric solar diagram analysis. The shading-affected data were excluded by retaining only periods when the solar azimuth (γ) lay outside the obstacle azimuth interval ([γA, γB]) and the solar elevation (α) exceeded the shading angle defined by αshadow = arctan(h / √(x² + y²)), where h is the height of the structure and the x and y are the distances of point A or B to the sensor. This method was also validated using an azimuth–solar elevation plot, where anomalous albedo values indicated the shading events calculated (see Fig. 2).

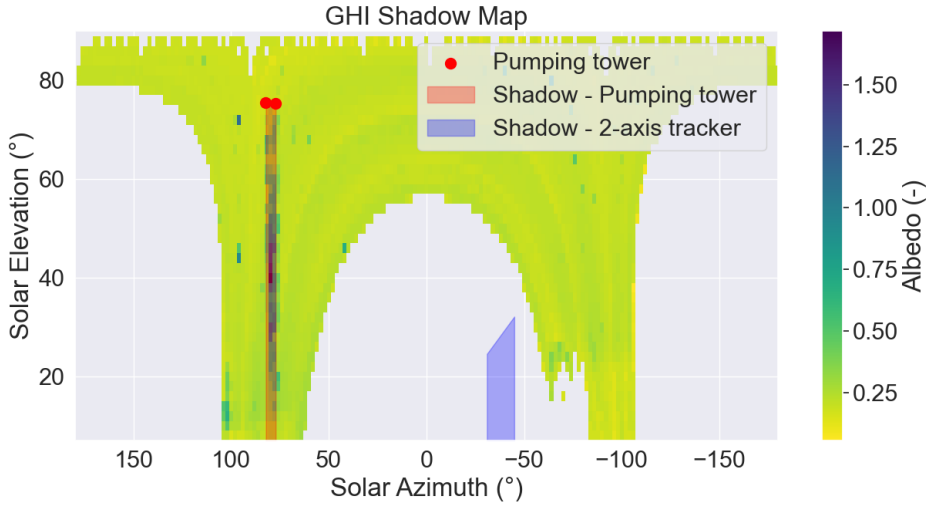

Fig. 2: Removal of shadow caused by experimental tower of a pumping system in the quality assurance procedure.

After data filtering, 64.9% of the diurnal measurements from 2025-02-07 to 2025-10-07 were retained. The global horizontal irradiance was decomposed into diffuse horizontal irradiance (DHI) and direct normal irradiance (DNI) using the Erbs and Starke3 models and the closure equation GHI = DHI + DNI cos(θz). These components, together with the measured reflected horizontal irradiance (RHI), were used to transpose the irradiance to the tilted plane using both the isotropic and HDKR models, adapted to estimate the rear and front irradiance.

Several metrics were used to assess the performance of the rear/front irradiances and their ratio for each model combination, including MBE, MAE and RMSE, their normalized values by the measurements mean, and the ratio of simulated to measured standard deviation (STDr).

After evaluating all irradiances and the rear-to-front ratio estimations, the bifacial gain simulated by each model combination was computed and compared to the measured scenario. The bifacial gain considered here is the percentage improvement captured by both sides with respect to a theoretical monofacial PV module which captures only GTI. The total irradiance incident on a theoretical bifacial PV module is computed by eq. 10.

$$G_{total} = GTI + \varphi\, RTI \quad \text{(eq. 10)}$$

Where φ is the bifaciality factor and G_{total} is the total incident irradiance. Typical values for the bifaciality factor are around 0.74 for p-type (PERC) and 0.81 for n-type modules TOPCon (Jang et al. 2023). More conservative values like 0.7 are commonly adopted in the literature (Ledesma et al., 2020). In the present work we adopted a bifaciality factor of 0.7.

4. Results

4.1. Horizontal and Tilted Rear/Front Ratio Measurements

Fig. 3 shows the dispersion plot and the average of the rear/front ratio in the horizontal and tilted planes. The horizontal rear/front ratio is in fact the global ground albedo. The sky dome diffuse irradiance captured by the backward tilted sensor leads to an increase in the average tilted rear/front ratio from 18.8% (horizontal) to 28.0% (tilted). For this reason, modelling the diffuse irradiance from the horizontal to the tilted plane is essential to ensure correct irradiance modelling in bifacial PV systems.

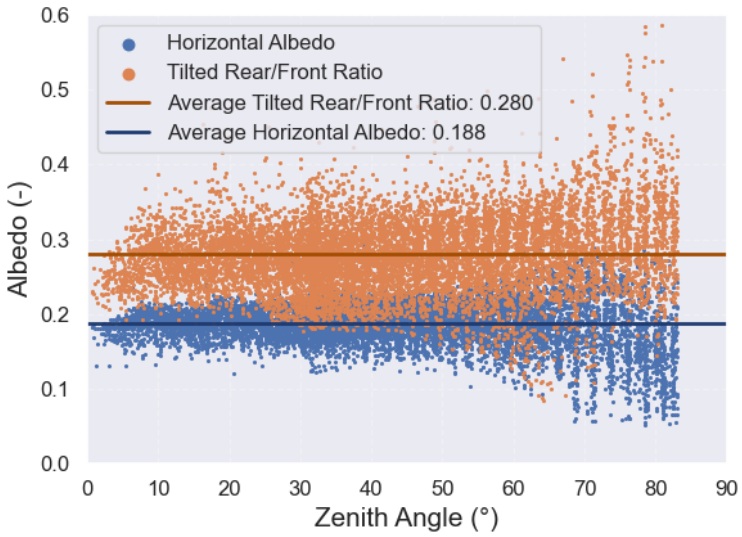

Fig. 3: Comparison of horizontal albedo and tilted rear/front ratio measurements.

4.2. Modelling Irradiance from Horizontal to Tilted Plane

Table 1 shows the performance results for the estimates of GTI (global tilted irradiance in front) and RTI (global tilted irradiance in the rear) for each model combination, with the best values for each metric highlighted in bold.

Tab. 1: Comparison of the GTI and RTI components obtained from the different radiation models.

	Sep.	Transp.	MAE (nMAE)	MBE (nMBE)	RMSE (nRMSE)	STDr
GTI (Mean: 465.9 W/m²)	Erbs	Isotropic	22.7W/m² (4.8%)	3.8W/m² (0.8%)	36.8W/m² (7.9%)	1.01
	Starke3		**21.1W/m² (4.5%)**	**0.2W/m² (0.0%)**	**35.3W/m² (7.5%)**	**1.00**
	Erbs	HDKR	26.7W/m² (5.7%)	9.2W/m² (2.0%)	40.7W/m² (8.7%)	1.02
	Starke3		22.9W/m² (4.9%)	5.9W/m² (1.3%)	37.1W/m² (7.9%)	1.01
RTI	Erbs	Isotropic	23.2W/m² (18.8%)	-23.2W/m² (-18.7%)	30.1W/m² (24.2%)	0.77
	Starke3		19.7W/m² (15.9%)	-19.6W/m² (-15.8%)	26.2W/m² (21.1%)	0.75

(Mean: 123.8 W/m²)	Erbs	HDKR	21.0W/m² (17.0%)	-20.6W/m² (-16.6%)	29.7W/m² (23.9%)	**0.82**
	Starke3		**17.1W/m² (13.8%)**	**-16.1W/m² (-13%)**	**25.2W/m² (20.3%)**	**0.82**

The Starke3 separation model demonstrates superior performance in estimating both GTI and RTI components. When paired with the Isotropic transposition model, this combination yields the most accurate results for GTI, as evidenced by the lowest values of nMAE, nMBE, nRMSE and STDr. These metrics collectively suggest that the Starke3 model provides a reliable estimation of solar irradiance, which is expected due to the high capacity to describe the diffuse fraction under high variability moments (see Fig 4).

In addition, RTI tends to be more difficult to estimate, with MAE errors in the same order of magnitude as GTI (around 17-26 W/m²), but a significantly higher normalized MAE. This happens due to a similar error magnitude (RTI nMAE of around 17~23W/m²) applied to a lower mean (RTI: 123.8 W/m²). In this sense, the RTI nMAE values can be up to 4.1 times higher than the GTI nMAE when adopting inaccurate model combinations, while they are around 3.06 times higher for the best performing combination. For the RTI estimations, the anisotropic model, specifically the HDKR model associated with Starke3 outperforms the Erbs associated with isotropic model by reducing the nMAE in 5% and providing simulated standard deviations closer to the measurements.

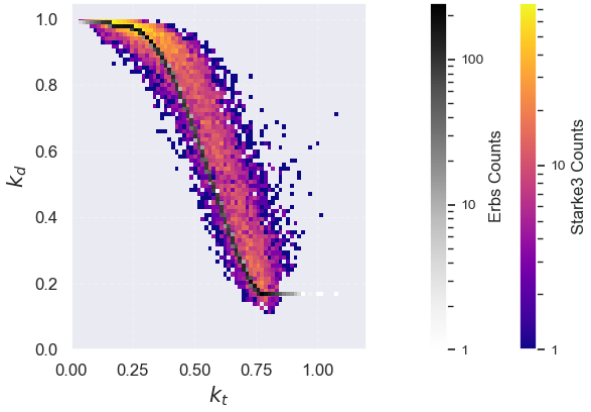

Fig. 4: Starke3 and Erbs diffuse fraction (k_d) under different sky conditions.

The accuracy gain of Starke3 on modeling RTI is also explained by the high levels of kd for intermediate to high kt levels, in these moments while Erbs underestimate the kd, Starke3 present higher horizontal diffuse irradiance impacting positively in the RTI calculations.

4.3 Comparison between Estimated and Measured Tilted Rear/Front Ratio

Fig. 5 shows the nMBE for different values of clearness index (k_t) and zenith angle.

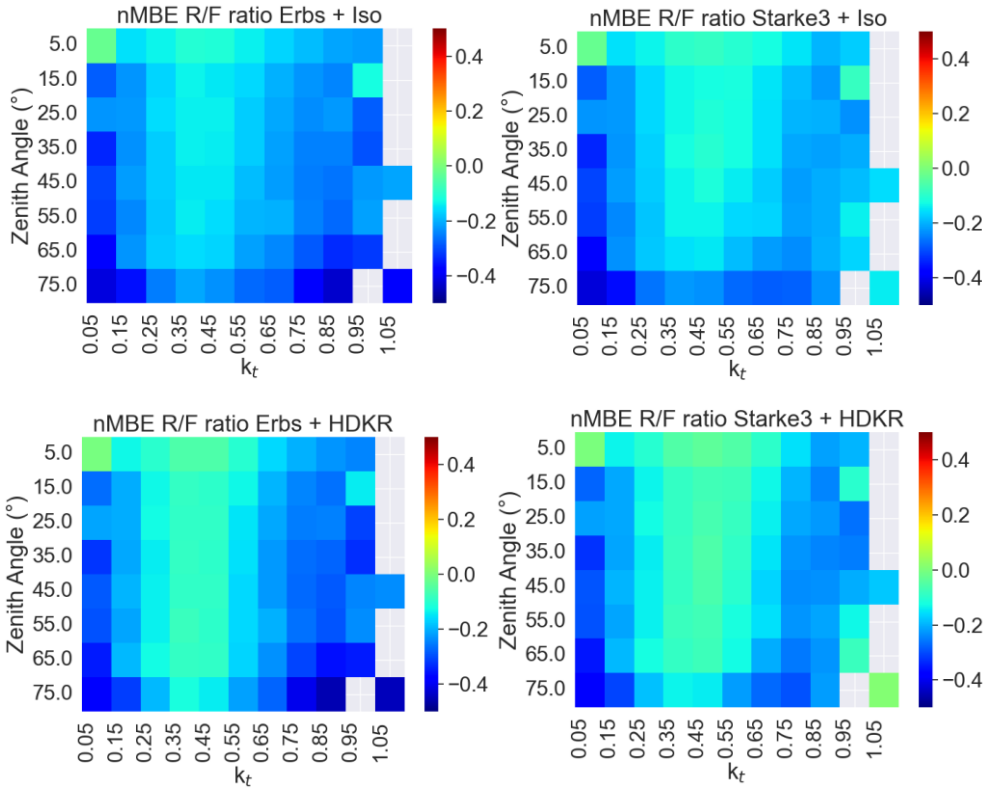

Fig. 5: Bias (nMBE) of the rear-to-front ratio for each range of kt and zenith angle values.

The adoption of the HDKR transposition model significantly improves the accuracy of rear/front (R/F) ratio estimates compared to the traditional isotropic approach. When combined with the Erbs decomposition, the HDKR model reduces the nRMSE from 24.2% to 22.1% (an improvement of approximately 9%), while with the Starke3 decomposition, the error decreases from 22.5% to 19.9% (around 12% improvement). Overall, the difference between the worst (Erbs + isotropic) and best (Starke3 + HDKR) combinations reaches around 18% in relative improvement for the nRMSE metric.

These results demonstrate that accounting for anisotropy and horizon brightening effects in the HDKR formulation leads to more consistent predictions under medium to high k_t conditions (see Fig. 5b and 5d). When combined with the multi-parameter Starke3 decomposition model, estimates show improved performance at high kt values, with nMBE approaching zero (green color), reflecting Starke3's superior ability for this problem compared to the simplified univariate Erbs model.

When evaluated by the average rear-to-front ratio, the model combinations yield estimates ranging from 22.2% (worst case: Erbs + Isotropic) to 23.8% (best case: Starke3 + HDKR), representing a 1.6% improvement between approaches. However, when compared to the measured average of 28.0%, all model combinations underestimate with deviations ranging from 15% to 21%. This indicates that while the selection of appropriate decomposition models significantly impacts prediction accuracy, substantial improvements in the sky and ground diffuse irradiance modeling are still required to fully capture the rear irradiance.

4.4 Bifacial Gain Estimation

An alternative way to understand the impact of modelling rear/front irradiance for bifacial systems is modelling the bifacial gain of the PV modules. As described in section 3, the bifacial gain is calculated for each model combination and measurement considering a theoretical conservative bifaciality factor of 0.7. Based on the total irradiance incident on the tilted plane of a PV module, Fig. 6 shows the difference between the measured bifacial gain of a theoretical bifacial PV module and the model combinations.

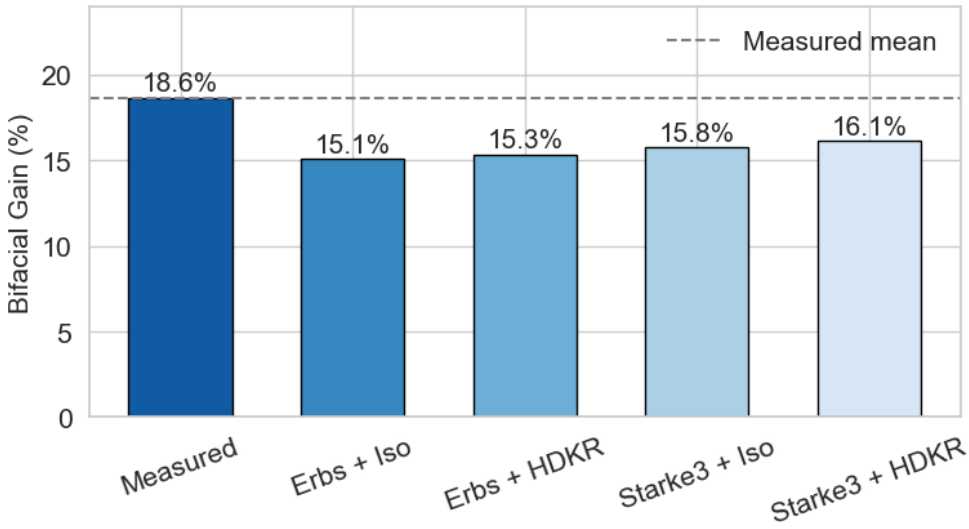

Fig. 6: Bifacial gain of each scenario (Measured and Simulated by different decomposition and transposition models). The theoretical bifacial gain is calculated based on the GTI and RTI for each specific scenario and a bifaciality factor of 0.7.

The bifacial gain analysis reinforces the underestimation observed in the rear/front ratio assessment. The measured bifacial gain of 18.6% significantly exceeds all model simulations, which range from 15.1% (Erbs + Isotropic) to 16.1% (Starke3 + HDKR), representing absolute deviations of 2.5 to 3.5 percentage points. Neglecting the anisotropic and horizon brightness irradiance components simulated by the Starke3 + HDKR model and adopting the simplest approach (Erbs and Isotropic) increases the bifacial gain estimation error by approximately 40%.

When compared to literature the theoretical bifacial gain obtained in this study (18.6%) is in line with those reported in other geographical locations. Johnson and Manikandan (2023) mapped bifacial system potential across India, a region with latitudes near the intertropical zone (between 8°N and 37°N), observing annual bifacial gains ranging between 2.5% and 22%.

5. Conclusions

This study demonstrated the high importance of diffuse irradiance modeling in the accurate estimation of rear/front ratios for bifacial photovoltaic systems. The comparative analysis of GHI decomposition models (Erbs and Starke3) and transposition models (Isotropic and HDKR) revealed significant differences in performance that directly impact bifacial system assessment.

The key findings indicate that the combination of the Starke3 decomposition model with the HDKR transposition model provides superior accuracy in estimating the rear irradiance component, reducing nRMSE by approximately 18% compared to the conventional Erbs + Isotropic approach. This enhanced performance of the Starke3 model stands for the incorporation of multiple meteorological variables, including the variability index and hourly clearness index, which better capture the temporal dynamics of atmospheric conditions. These characteristics optimize the irradiance modelling particularly under medium to high clearness index conditions.

The research confirms that diffuse irradiance captured by tilted surfaces plays a fundamental role in determining the rear-to-front ratio and consequently the bifacial gain with implications extending beyond simple geometric considerations. The anisotropic nature of sky radiance distribution, as captured by the HDKR model, proves essential for accurate rear irradiance estimation and consequently, rear-to-front ratio and bifacial gain estimation. Furthermore, the study highlights the limitations of simplified isotropic approaches when applied to bifacial systems, where the accurate characterization of TDRs becomes critical for reliable performance predictions.

Future research should focus on evaluating the impact of different ground and sky modelling and albedo modelling across different geographical locations and climatic conditions. Additionally, the implementation and validation of alternative tilted diffuse models for bifacial modules, including explicit treatment of module shading effects on ground-reflected irradiance, represents an important direction for improving prediction

accuracy.

6. Acknowledgments

We extend our sincere gratitude to the Coordination for the Improvement of Higher Education Personnel – Brazil (CAPES) for their funding and invaluable support for the Postgraduate Program at UFPE. Additionally, we are grateful to the São Francisco Hydroelectric Company (CHESF-ELETROBRAS) for their support through the CHESF-CASANOVA project, ANEEL CODE: PD-00048-0217.

7. References

Asgharzadeh, A., Abou Anoma, M., Hoffman, A., Chaudhari, C., Bapat, S., Perkins, R., Bourne, B., 2019. A benchmark and validation of bifacial PV irradiance models. In: Proceedings of the 46th IEEE Photovoltaic Specialists Conference (PVSC), pp. 3281–3287. IEEE. https://doi.org/10.1109/PVSC40753.2019.8981188

Deline, C., Ovaitt, S., Gostein, M., Braid, J., Newmiller, J., Suez, I., 2024. Irradiance monitoring for bifacial PV systems' performance and capacity testing. IEEE Journal of Photovoltaics. https://doi.org/10.1109/JPHOTOV.2024

Durusoy, B., Ozden, T., Akinoglu, B.G., 2020. Solar irradiation on the rear surface of bifacial solar modules: a modeling approach. Scientific Reports 10, 13300. https://doi.org/10.1038/s41598-020-70231-4

Erbs, D. G., Klein, S. A., & Duffie, J. A. (1982). Estimation of the diffuse radiation fraction for hourly, daily and monthly-average global radiation. Solar energy, 28(4), 293-302.

Ineichen, P., 2008. A broadband simplified version of the Solis clear sky model. Solar Energy 82, 758–762. https://doi.org/10.1016/j.solener.2008.02.009

Jang, H., Lee, S., Lee, H., Choi, D., Song, H., Jeong, J., Kang, Y., 2024. Comparative study on energy yield of tunnel oxide passivated contact (TOPCon) and passivated emitter and rear contact (PERC) solar cells and analysis of optimal installation method for vertical photovoltaics. Process Integration and Optimization for Sustainability 8(4), 993–1001. https://doi.org/10.1007/s41660-024-00475-1 Johnson, J., Manikandan, S., 2023. Resource potential mapping of bifacial photovoltaic systems in India. iScience 26(10), 108266. https://doi.org/10.1016/j.isci.2023.108266

Ledesma, J.R., Almeida, R.H., Martinez-Moreno, F., Rossa, C., Martín-Rueda, J., Narvarte, L., Lorenzo, E., 2020. A simulation model of the irradiation and energy yield of large bifacial photovoltaic plants. Solar Energy 206, 522–538. https://doi.org/10.1016/j.solener.2020.06.027

Liu, B., Jordan, R., 1961. Daily insolation on surfaces tilted towards equator. ASHRAE J., 10.

Marion, B., MacAlpine, S., Deline, C., Asgharzadeh, A., Toor, F., Riley, D., Hansen, C., 2017. A practical irradiance model for bifacial PV modules. In: Proceedings of the 44th IEEE Photovoltaic Specialists Conference (PVSC), Washington, D.C., pp. 1537–1542. IEEE. https://doi.org/10.1109/PVSC.2017.8366730

McArthur, L., 2005. Baseline Surface Radiation Network (BSRN) Operations Manual. TD-No. 1274, WCRP/WMO, World Meteorological Organization, Geneva.

Petribú, L., Sabino, E.R., Barros, H., Costa, A., Barbosa, E., Castro Vilela, O.D., 2017. Procedimento objetivo para a garantia de qualidade de dados de radiação solar. Avances en Energías Renovables y Medio Ambiente 21, 67–78.

Reindl, D. T., Beckman, W. A. and Duffie, J. A.. 1990. Evaluation of Hourly Tilted Surface Radiation Models. SolarEnergy, 45(1), 9–17

Ridley, B., Boland, J., e Lauret, P., 2010. Modelling of diffuse solar fraction with multiple predictors. Renewable Energy, 35(2), 478-483

Rodríguez-Muñoz, J.M., Alonso-Suárez, R., Bove, I., Abal, G., 2024. Assessing the impact of diffuse fraction estimation on ground albedo modeling. In: Eurosun2024, Limassol, Cyprus.

Starke, A. R., Lemos, L. F., Boland, J., Cardemil, J. M. and Colle, S., 2018. Resolution of the cloud enhancement problem for one-minute diffuse radiation prediction. Renewable Energy, 125, 472-484.

Starke, A. R., Lemos, L. F., Barni, C. M., Machado, R. D., Cardemil, J. M., Boland, J. and Colle, S., 2021. Assessing one-minute diffuse fraction models based on worldwide climate features. Renewable Energy, 177, 700-714

Sun, X., Khan, M.R., Deline, C., Alam, M.A., 2018. Optimization and performance of bifacial solar modules: a global perspective. Applied Energy 212, 1601–1610. https://doi.org/10.1016/j.apenergy.2017.12.041

VDMA, 2024. International Technology Roadmap for Photovoltaic (ITRPV), 15th Edition. VDMA, Frankfurt am Main. Available at: https://itrpv.vdma.org

Ward, G. J. 1994. The RADIANCE Lighting Simulation and Rendering System. Proceedings of the 21st Annual Conference on Computer Graphics and Interactive Techniques, ACM.